Emulating Ray-Tracing Channels in Multi-probe Anechoic Chamber Setups for Virtual Drive Testing

Fan, Wei; Llorente, Ines Carton; Kyösti, Pekka; Pedersen, Gert F.

Published in:
I E E E Transactions on Antennas and Propagation

DOI (link to publication from Publisher):
10.1109/TAP.2015.2498951

Publication date:
2016

Emulating Ray-Tracing Channels in Multi-probe Anechoic Chamber Setups for Virtual Drive Testing

Wei Fan, Ines Carton, Pekka Kyösti and Gert F. Pedersen

***Abstract*—This paper discusses virtual drive testing (VDT) for multiple-input multiple-output (MIMO) capable terminals in multi-probe anechoic chamber (MPAC) setups. We propose to perform VDT, via reproducing ray tracing (RT) simulated channels with the field synthesis technique. Simulation results demonstrate that, realistic RT channels can be accurately reproduced within the test zone with a limited number of probes in MPAC setups. The feasibility of performing VDT via reproducing RT simulated channels is supported by measurement results in a practical 3D MPAC setup. The amplitude and phase of the electric field have been measured throughout the test zone with a calibration dipole, and excellent match between the simulation and measurement was achieved.**

***Index Terms*—Virtual drive testing, ray tracing simulation, array synthesis, field synthesis validation, multi-probe anechoic chamber setup, MIMO OTA testing.**

I. Introduction

Drive test, where mobile terminals are evaluated in a live network, is mandatory before massive device roll-out. It is required in the stage of device troubleshooting, performance evaluation and regression testing. However, it is expensive, time-consuming and labor-intensive. Furthermore, due to open-air testing environments, drive testing might be unrepeatable and uncontrollable. The concept of virtual drive test (VDT) has attracted great interest in industry recently [1]–[3], where the basic idea is to bring drive testing in a controllable environment. That is, propagation channels are recorded along drive routes during a drive test and then reproduced in the laboratory. Mobile terminals are connected to base stations (or base station emulators) and their performance is evaluated under the recorded channels in laboratory conditions. VDT is attractive, as testing is performed in an automated, controllable and repeatable manner. Moreover, VDT can significantly reduce the test time, work load and cost. The main challenge lies in reproducing the same propagation environments as the device would experience during a drive test in a controlled environment.

Over the air (OTA) testing methods of multiple-input multiple-output (MIMO) and diversity capable terminals are under discussion in standards [4]. Antennas are considered inherently in the OTA testing. Several OTA systems have been proposed to evaluate MIMO capable terminals [4], e.g. two stage systems (with conducted/radiated two-stage methods), reverberation chamber based systems (with/without a radio channel emulator), multi-probe anechoic chamber (MPAC) based systems (with 2D/3D probe configurations), and etc. An overview of the capabilities and challenges in MPAC systems for MIMO OTA testing was presented in [5]. The MPAC method is a promising solution for VDT, due to its potential to physically reproduce arbitrary multipath environments in the laboratory [5], [6].

The focus of research work in MPAC setups is mainly on how to reproduce geometry-based stochastic channel (GBSC) models with a limited number of probes [4], [7]. Algorithms implemented in commercial channel emulators are limited to reproduce GBSC models in MPAC setups [7], [8]. Cluster-based channel models, though well-accepted and standardized, might fall short of achieving VDT, as GBSCs are not site-specific and assumed stationary within a single drop (i.e. a snapshot of fading channels) [9]. Furthermore, GBSCs would fail to model realistic dynamic channels, as different drops are realized randomly. Deterministic channel models, which characterize the physical propagation parameters in a deterministic manner (e.g. ray tracing (RT) simulations and recorded measurement data), are desirable for performing VDT. The idea of replaying recorded channel data from a live network in MPAC setups was briefly mentioned in [10], where the basic idea is to reconstruct cluster-based channel models based on the recorded data. In [11], recorded multipath channels are reproduced in a 3D MPAC setup using spherical-wave theory. However, recording channel data for VDT requires accurate channel sounding measurements in various scenarios, and expensive channel sounding equipment. In this paper, we propose to perform VDT in MPAC setups, via reproducing RT simulated channels. RT channels are reproduced based on field synthesis technique in MPAC setups. RT simulation has been widely used to predict site-specific and location-dependent radio channels [12], [13]. Furthermore, due to the high accuracy and adherence to the actual propagation mechanism, RT simulations are often used as an alternative to replace field measurements to save the time and complexity required by actual measurements [14].

The main contributions of the paper are listed as follows:

- The concept of performing VDT by replaying RT channels in MPAC setups is introduced in Section III. This method is cost-effective and realistic, and hence can be used for design, development and testing multiple antenna systems. Simulation results in Section IV demonstrate that, RT channels can be accurately reproduced within the test zone with a limited number of probes.
- A method based on field synthesis is described in Sec-

Wei Fan, Ines Carton, and Gert F. Pedersen are with the Antennas, Propagation and Radio Networking section at the Department of Electronic Systems, Faculty of Engineering and Science, Aalborg University, Denmark (email: {wfa, icl, gfp}@es.aau.dk).

Pekka Kyösti is with Anite Telecoms Oy, Oulu, Finland (email: {pekka.kyosti}@anite.com).

tion III to reproduce rays characterized by arbitrary complex amplitudes, impinging angles (azimuth and elevation) and polarizations (linear, circular and elliptical) in MPAC setups.

- Measurement results presented in Section V validate the field synthesis technique for the first time in a practical 3D MPAC setup, to the best knowledge of the authors. Excellent agreement between measured and simulated complex field was achieved. The feasibility of performing VDT via reproducing RT simulated channels is supported by measurements in a practical 3D MPAC setup.

II. Ray Tracing channels

RT method predicts electromagnetic field at the receiver (Rx) due to an energy source at the transmitter (Tx) based on a collection of theories including geometry optics, uniform theory of diffraction and other scattering mechanisms. RT models are used in the planning phase of mobile radio systems to save deployment cost and increase service quality.

A 3D RT tool "3D Scat", implemented by Bologna University [12] was used in the study. The RT tool models the usual deterministic propagation mechanisms, i.e. transmission, reflection, and diffraction both from lateral walls or edges and from over-roof-top propagation. Moreover, it further enriches the propagation model by including diffuse scattering due to building wall roughness or irregularities, and back-scattering from far objects. Diffuse scattering has been shown to have an impact on the temporal characteristics and the angular dispersion of the channel [12], [13], [15], and therefore it will impact MIMO performance. The diffuse scattering model employed by the tool is described in [15].

The RT tool allows to define a scenario composed of prisms that represent buildings or other obstacles. One or more Tx can be defined, which are characterized by their positions, antenna radiation characteristics, frequency of operation, and transmit power. Similarly, one or more Rx can be defined according to their positions and antenna radiation characteristics. Then, a combination of image RT and diffuse scattering is used to simulate the rays departing from each of the Tx and arriving to each of the Rx, as described in [12]. The tool allows to predefine a maximum number of interactions, i.e. reflections, diffractions, or scattering; and to limit the minimum power of a single ray, thus allowing to limit the total number of rays and simulation complexity. The output of simulations consists of the propagation trajectory, AoD, AoA, delay, vectorial electrical field, polarization, and received power for each ray. Figure 1 shows an example scenario, where the rays from one Tx to two different Rx positions are illustrated.

With the output values from the RT tool, the channel impulse response at the ith Rx position h_i, can be expressed as a sum of all rays arriving to the i Rx position:

$$h_i(\tau,\theta,\phi) = \sum_{q=1}^{Q} \vec{E}_q \cdot \delta(\tau-\tau_q)\delta(\theta-\theta_q)\delta(\phi-\phi_q) \qquad (1)$$

where Q is the total number of rays arriving to the i Rx position, and τ_q, θ_q, ϕ_q, and $\vec{E}_q$ are the delay, elevation AoA, azimuth AoA, and vectorial complex field of the q-th ray,

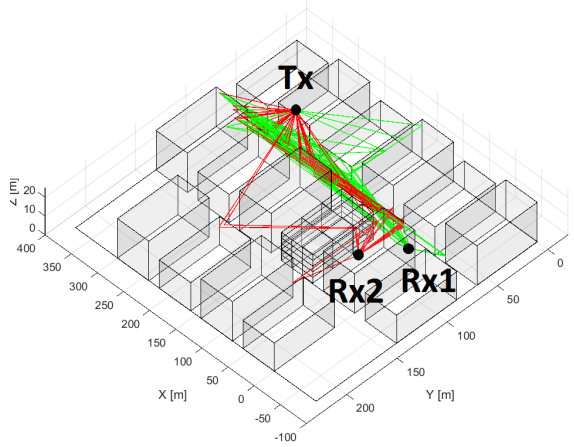

Figure 1. 3D ray tracing scenario with one Tx, and two Rx positions. Green lines represent rays from Tx to Rx position 1, and red lines represent rays from Tx to Rx position 2.

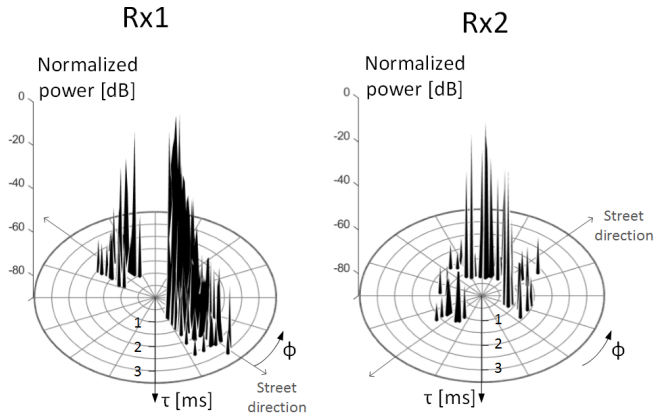

Figure 2. Power-azimuth-delay spectrum for two Rx positions. Power is normalized with respect to its maximum, and delay is represented in the radial direction. Street direction is indicated by grey arrows.

respectively. Note that the focus is on reproducing the AoAs, complex field and polarizations of the rays, while the delay generation is a trivial task with a digital channel emulator.

Figure 2 shows the power-azimuth-delay spectrum simulated with the RT tool for the two Rx positions shown in Figure 1. Rx 1 is in a LOS scenario, while the LOS path is blocked for Rx 2. For Rx 1, the street canyon effect can be clearly observed, where all the rays are reaching Rx position 1 from the direction of the street, as shown in Figure 2 (left). Rays impinging Rx 2 have a wider range of azimuth angles, as Rx 2 is placed relatively close to the street corner, where the rays are diffracted. Figure 2 also represents an example of two Rx positions that would experience completely different propagation environments, though closely located. Realistic and dynamic propagation conditions can be simulated using the RT tool, where the non-stationary characteristics of the environment can be captured.

III. 3D Field Synthesis in MPAC setups

A. VDT in MPAC setups

A MPAC system mainly consists of a base station emulator, a channel emulator and multiple probe antennas located around

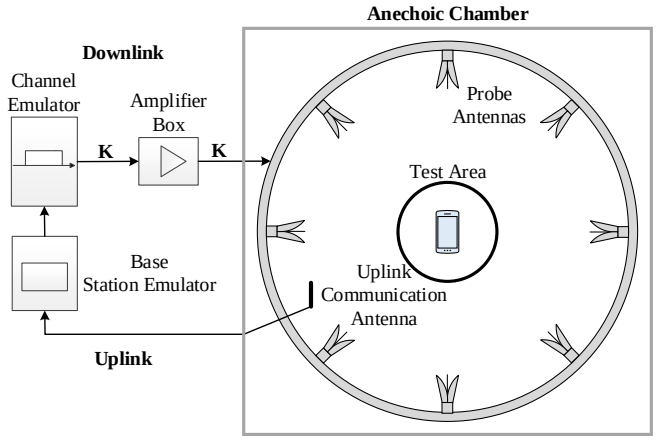

Figure 3. Channel emulation in the MPAC setups. For validation measurements, the base station emulator is replaced by a vector network analyzer (VNA), and a calibration antenna connected to the VNA. The position of the calibration antenna is controlled to scan the field inside the test zone.

a device under test (DUT) inside an anechoic chamber, as shown in Figure 3. The test zone is a geometric area in the center of MPAC setups where desired propagation channels can be accurately reproduced. The antenna separation on the DUT should be smaller than the test zone size to ensure that the DUT is evaluated under the desired channel conditions. Different channel emulators used in MPAC setups have been shown in the literature, e.g. commercial channel emulators [1], [3], and a multipath simulator based on phase shifters, attenuators and delay lines [16], [17]. As the key idea of VDT in this paper is to reproduce RT channels based on field synthesis, it is beneficial to have a channel emulator that is capable of file-based emulation. Furthermore, amplitude and coherent phase control at the channel emulator's output ports are required for field synthesis purpose.

A driving route can be represented by a sufficient number of Rx positions in the RT tool. For each Rx position a collection of rays characterized by their complex amplitudes, polarizations, delays and AoAs can be calculated using the "3D Scat" ray tracing tool, as explained in Section II. The main idea is to reproduce the rays generated by the RT tool in a 3D MPAC setup for each Rx position. The DUT is placed in the center of the setup and the time-variant propagation channels are emulated by reproducing channels along the simulated Rx route with a replay rate that corresponds to the Rx moving speed along its route in the channel emulator.

B. Field synthesis using antenna arrays

Field synthesis using antenna arrays has been intensively investigated for testing single antenna systems and electromagnetic-susceptibility testing of electronic devices [18]–[20]. The target is to achieve a plane wave along the antenna aperture, which is inherently assumed to be linearly polarized. Recently, plane wave synthesis has been considered to reproduce radio channels in MPAC setups for testing multiple antenna systems. To mimic multipath propagation environments, waves with arbitrarily impinging angles and arbitrary polarizations are expected in channel emulation. The test zone for multiple antenna systems is a geometrical area which encloses the DUT (i.e. a 3D volume).

Generation of vertically polarized plane waves with arbitrary impinging angles in MPAC setups was firstly described in [7]. Field synthesis in a 3D MPAC setup is discussed in [21], although no algorithm description was given. In [22], field synthesis in a hemisphere MPAC setup was discussed. However, it was not described how wave polarization was considered in the algorithm. In [23], appropriate 3D probe configurations were discussed as well, though no details on the algorithm were given.

C. 3D field synthesis in MPAC setups

In this part, the field synthesis technique to emulate rays with arbitrary complex amplitudes, polarizations, and AoAs is discussed. The discussion is firstly focused on a single ray and later extended to RT simulated channels.

A 3D MPAC setup is shown in Figure 4, where each OTA probe is dual-polarized and pointed to the sphere center. Assume the MPAC setup consists of K probes located at $\bar{p}_k = [x_k^p, y_k^p, z_k^p]^T$ with $k = 1, ...K$ and the test zone is sampled by M points, located at $\bar{s}_m = [x_m^s, y_m^s, z_m^s]^T$ with $m = 1, ...M$, where $()^T$ denotes the transpose operator.

1) Target ray: Assume that a ray with planar wavefront and wave vector $\bar{\beta}$ is targeted, as shown in Figure 5. An ideal plane wave is characterized by uniform amplitude distribution over the test zone and linear phase front along the propagation direction $\bar{\beta}$. The target field at sample point m is:

$$e_m = E_o \exp(-j\bar{\beta} \cdot \bar{s}_m), \tag{2}$$

where E_o is constant for all samples over the test zone and $||\bar{\beta}|| = 2\pi/\lambda$.

The polarization of the target electric fields and emulated electric fields radiated from the probes are defined in different local coordinate systems. To ensure that the emulated field matches with the target field in terms of complex amplitude and polarization, both the target field and emulated field should be transformed in to the same global coordinate system with three orthogonal basis vectors $\bar{x}$, $\bar{y}$ and $\bar{z}$, as illustrated in Figure 5. For a target ray with wave vector $\bar{\beta}$, the electrical fields can be transformed into the global coordinate systems as:

$$\begin{bmatrix} e_m^x \\ e_m^y \\ e_m^z \end{bmatrix} = e_m \cdot A \begin{bmatrix} w_\theta \\ w_\phi \\ 0 \end{bmatrix}, \tag{3}$$

where $\mathbf{e}^x = [e_1^x, ...e_M^x]^T$, $\mathbf{e}^y = [e_1^y, ...e_M^y]^T$ and $\mathbf{e}^z = [e_1^z, ...e_M^z]^T$ are the target electric field vectors for the M sample points in $\bar{x}$, $\bar{y}$ and $\bar{z}$ directions in the global coordinate, respectively. A is the coordinate transformation matrix from the spherical coordinate with basis vectors $\bar{\theta}$, $\bar{\phi}$ and $\bar{\beta}$ to the global coordinate with basis vectors $\bar{x}$, $\bar{y}$ and $\bar{z}$, as shown in Figure 5. w_θ and w_ϕ are the complex amplitudes assigned to the θ polarized and ϕ polarized field, respectively. Note that arbitrarily polarized rays can be obtained by properly setting w_θ and w_ϕ.

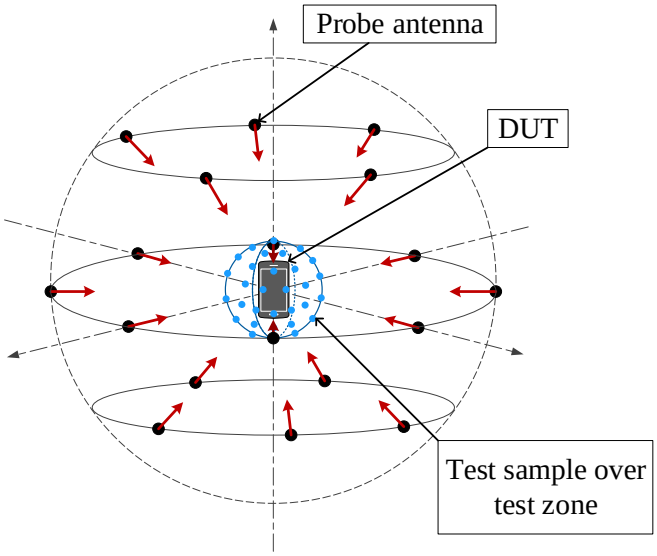

Figure 4. An illustration of a 3D MPAC setup. Probes (marked with black dots) are dual polarized and pointed towards the center. Samples over the test area are marked with blue circles.

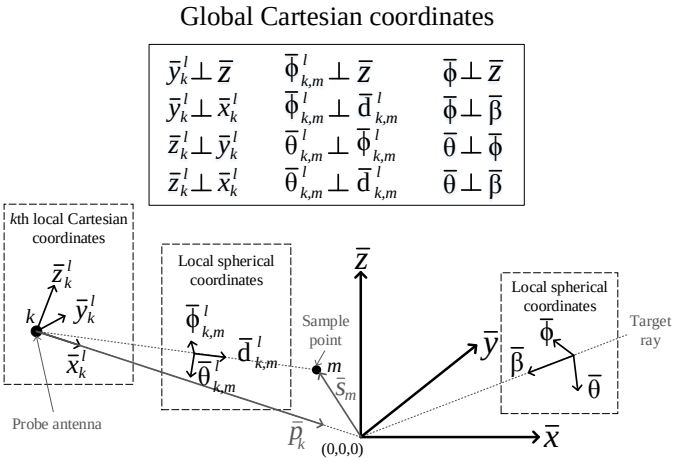

Figure 5. An illustration of the coordinate systems. Polarization is defined in the local coordinate system., e.g. for the target ray defined with local spherical coordinates ($\bar{\beta}$,$\bar{\theta}$,$\bar{\phi}$), vertical polarization refers to the polarization along $\bar{\theta}$, whereas horizontal polarization refers to the polarization along $\bar{\phi}$.

2) Synthesized ray: The propagation coefficient from the kth probe to the mth sample location is:

$$\alpha_{m,k} = \frac{\lambda}{4\pi||\bar{d}_{k,m}||} \exp(-j||\bar{\beta}|| \cdot ||\bar{d}_{k,m}||), \tag{4}$$

where $||\bar{d}_{k,m}|| = ||\bar{p}_k + \bar{s}_m||$ is the propagation distance from the kth probe to the mth sample.

The synthesized field at the mth point in the kth local coordinate system can be written as:

$$\begin{bmatrix} \hat{e}^{x,l}_{k,m} \\ \hat{e}^{y,l}_{k,m} \\ \hat{e}^{z,l}_{k,m} \end{bmatrix} = \alpha_{m,k} \cdot A^l_{k,m} \begin{bmatrix} g^{\theta}_k \\ g^{\phi}_k \\ 0 \end{bmatrix}, \tag{5}$$

where $\hat{\mathbf{e}}^{x,l}_k = [\hat{e}^{x,l}_{k,1}, ..., \hat{e}^{x,l}_{k,M}]$, $\hat{\mathbf{e}}^{y,l}_k = [\hat{e}^{y,l}_{k,1}, ..., \hat{e}^{y,l}_{k,M}]$ and $\hat{\mathbf{e}}^{z,l}_k = [\hat{e}^{z,l}_{k,1}, ..., \hat{e}^{z,l}_{k,M}]$ are the synthesized electric field vectors at the M sample points in $\bar{x}^l_k$, $\bar{y}^l_k$ and $\bar{z}^l_k$ directions in the kth local coordinate, respectively. $A^l_{k,m}$ is the transformation matrix from the kth local spherical coordinate characterized by $\bar{\theta}^l_{k,m}$, $\bar{\phi}^l_{k,m}$, and $\bar{d}^l_{k,m}$ to the kth local Cartesian coordinate characterized by $\bar{x}^l_k$, $\bar{y}^l_k$ and $\bar{z}^l_k$. $\mathbf{g}^{\theta} = \{g^{\theta}_k\}$ and $\mathbf{g}^{\phi} = \{g^{\phi}_k\}$ are the complex amplitude weight vectors to be optimized for the θ and ϕ polarized ports, respectively. The synthesized field at the mth point at the global coordinate can be written as:

$$\begin{bmatrix} \hat{e}^{x}_{m} \\ \hat{e}^{y}_{m} \\ \hat{e}^{z}_{m} \end{bmatrix} = \sum_{k=1}^{K} B^T_k \cdot \begin{bmatrix} \hat{e}^{x,l}_{k,m} \\ \hat{e}^{y,l}_{k,m} \\ \hat{e}^{z,l}_{k,m} \end{bmatrix}, \tag{6}$$

where $\hat{\mathbf{e}}^{x} = [\hat{e}^{x}_1, ...\hat{e}^{x}_M]^T$, $\hat{\mathbf{e}}^{y} = [\hat{e}^{y}_1, ...\hat{e}^{y}_M]^T$ and $\hat{\mathbf{e}}^{z} = [\hat{e}^{z}_1, ...\hat{e}^{z}_M]^T$ are the synthesized electric field vectors for the M sample points in $\bar{x}$, $\bar{y}$ and $\bar{z}$ directions in the global coordinate, respectively. B_k is the transformation matrix from the kth local coordinate characterized by three orthogonal basis vectors $\bar{x}^l_k$, $\bar{y}^l_k$ and $\bar{z}^l_k$ to the global coordinate.

3) Objective function: The goal is to obtain complex weights $\mathbf{g}^{\theta}$ and $\mathbf{g}^{\phi}$ for the θ and ϕ polarized ports of the probes that minimize the deviation between the theoretical electric fields and the synthesized electric fields over the M sample points. To minimize the summation over the total emulation error, the objective function can be written as:

$$\min_{\mathbf{g}^{\theta},\, \mathbf{g}^{\phi}} \left\| \begin{bmatrix} \hat{\mathbf{e}}^{\boldsymbol{x}} \\ \hat{\mathbf{e}}^{\boldsymbol{y}} \\ \hat{\mathbf{e}}^{\boldsymbol{z}} \end{bmatrix} - \begin{bmatrix} \mathbf{e}^{\boldsymbol{x}} \\ \mathbf{e}^{\boldsymbol{y}} \\ \mathbf{e}^{\boldsymbol{z}} \end{bmatrix} \right\|^2_2 \tag{7}$$

Equation (7) is a convex problem, which can be handled efficiently. The surface of the test volume needs to be sampled with sufficient samples (with M larger than K) to ensure that the simulation accuracy inside the surface is good. According to Huygens's principle [24], provided the synthesized field on a closed surface is equal to the target field, the electric field inside the closed surface would be accurately synthesized.

4) Emulating multiple rays: Assume we have Q rays impinging the test zone, (7) can be used to calculate the complex weights $g^{\theta}_{k,q}$ and $g^{\phi}_{k,q}$ for the θ and ϕ polarized ports of the kth probe for each ray q. It might be computationally heavy to calculate weights for a high number of target rays. In the actual generation of impulse response data, the weights could be taken from a pre-calculated table to reduce computational time.

5) Figure of merit: To evaluate how well the synthesized field matches the target field for a single plane wave, amplitude quality factor and phase quality factor are often used [25] [26]. However, quality factors are not defined to evaluate multiple plane waves. In this paper, the error vector magnitude (EVM) is used to determine the field synthesis accuracy [22]. For the mth sample point in the test zone, we have:

$$\mathrm{EVM}_m = 10 \cdot \log \left\{ \frac{|(e^x_m - \hat{e}^x_m)|^2 + |(e^y_m - \hat{e}^y_m)|^2 + |(e^z_m - \hat{e}^z_m)|^2}{|e^x_m|^2 + |e^y_m|^2 + |e^z_m|^2} \right\} \tag{8}$$

The maximum and root mean square (rms) EVM over the total M samples on the test zone surface is used in the simulation results below. Note that the EVM inside the test zone surface will be smaller, according to Huygen's principle.

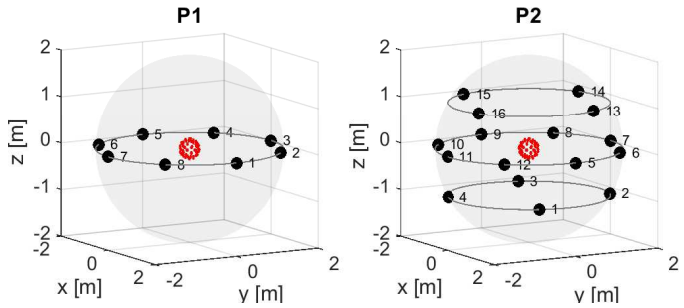

Figure 6. Probe configurations considered in the simulations. P1: $K = 8$ uniformly distributed probe antennas on a 2D OTA ring with 45^o step. P2: $K = 16$ probes placed on three elevation rings with elevation angles 30^o, 0^o and -30^o, respectively. For the two elevation rings, 4 probes with azimuth angles from -45^0 to 45^0 with 90^0 step are used, while 8 probes placed as in P1 is used for the azimuth ring. OTA sphere radius is set to 2 m.

Table I
SCENARIOS FOR SINGLE RAY EMULATION.

Scenario	Angle	Polarization	Setup	rms EVM
A	AoA = 22.5^o EoA=0^o	Circular	P1	-20.8 dB
B	AoA = 22.5^o EoA=0^o	Circular	P2	-21.3 dB
C	AoA = 22.5^o EoA=15^o	Circular	P2	-20.6 dB

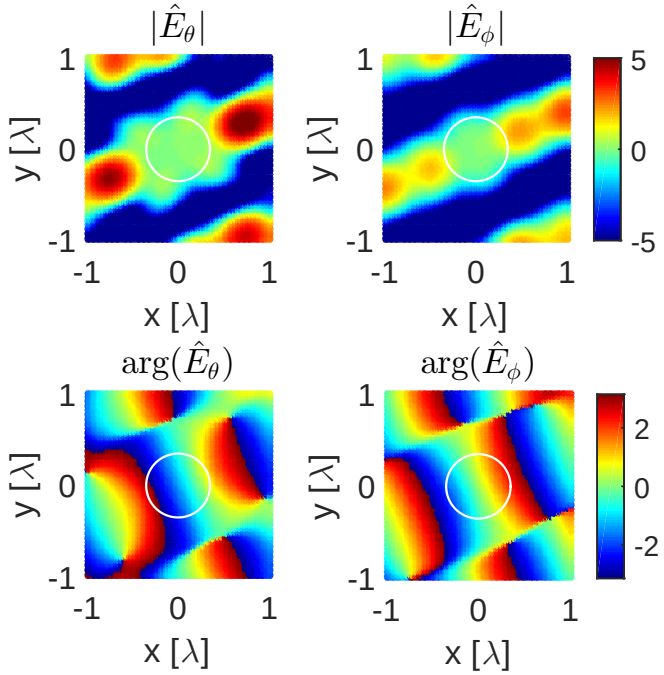

Figure 7. $\hat{E}_\theta$ and $\hat{E}_\phi$ for scenario A on the azimuth plane. Top: Field strength [dB]. Bottom: phase [rad]. Circle denotes the test zone on azimuth plane.

IV. SIMULATION RESULTS

To illustrate how well the algorithm proposed in Section III-C works, two probe configurations are considered in the simulations, as shown in Figure 6. The test area diameter is set to 0.7 λ. The sample points on the surface of the test area are selected according to a Lebedev distribution to approximate a uniform distribution on a sphere. Two simulation scenarios are considered: 1) single ray emulation for validation of concept, and 2) RT channel emulation.

A. Single ray emulation

The target scenarios considered in the simulations are detailed in Table I. We examine a set of representative yet challenging target rays, e.g. a target ray impinging from between two adjacent probes in scenario A. The emulated vertically polarized field $\hat{E}_\theta$ and horizontally polarized field $\hat{E}_\phi$ over the azimuth plane (with elevation angle 0^o) for scenario A are shown in Figure 7. Uniform power over the test area and linear phase front along the propagation direction (i.e. 22.5^o) can be observed for both polarizations. Furthermore, the ray polarization is accurately modeled, since $\hat{E}_\theta$ and $\hat{E}_\phi$ have a phase difference of 90^o and equal amplitude at test zone center.

The EVM for scenario A over the azimuth plane is shown in Figure 8 (top left). The rms EVM over the samples on the circle is -21dB, indicating high emulation accuracy in the azimuth plane. The rms EVM in the plane perpendicular to the ray direction is shown in Figure 8 (top right). The accuracy deteriorates along elevation as expected, since all probes are located on the azimuth plane. The EVM for scenario B over the mentioned planes is shown in Figure 8 (below). A slight improvement of the EVM over elevation can be observed, compared to scenario A. This is due to the fact that a 3D configuration is used instead.

The emulated vertically polarized field $\hat{E}_\theta$ and horizontally polarized field $\hat{E}_\phi$ for scenario C are shown in Figure 9. The amplitude distributions are uniform over the test area on the perpendicular plane, as expected. Furthermore, linear phase front can be observed on the perpendicular plane for both polarizations. The ray polarization is well modeled, as we can see from Figure 9. The rms EVM values calculated from the samples on surface of the test zone for different scenarios are shown in Table I.

B. RT channel emulation

1) RT simulation: A simplified urban scenario is selected for the RT simulation, shown in Figure 10. Buildings with different heights are represented in gray. The Tx is located on top of a building. Two routes are simulated, as shown in Figure 10. Route 2 is closer to the Tx antenna, thus the received rays are expected to have higher elevation angles than for Route 1. Line of sight (LOS) and non-LOS (NLOS) scenarios are considered in both routes. For the sake of simplicity, both routes are 20 m long and the routes are sampled with 21 equally spaced Rx positions (i.e. 1 m separation between Rx positions). The first 10 Rx samples are in the NLOS region, whereas the rest are in the LOS region. The direction of travel is represented in the figure with arrows. Note that realistic scenarios with many more Rx sample points could be considered with the proposed algorithms as well.

The power angular spectrum in azimuth and elevation along the two routes are shown in Figure 11. For the LOS region

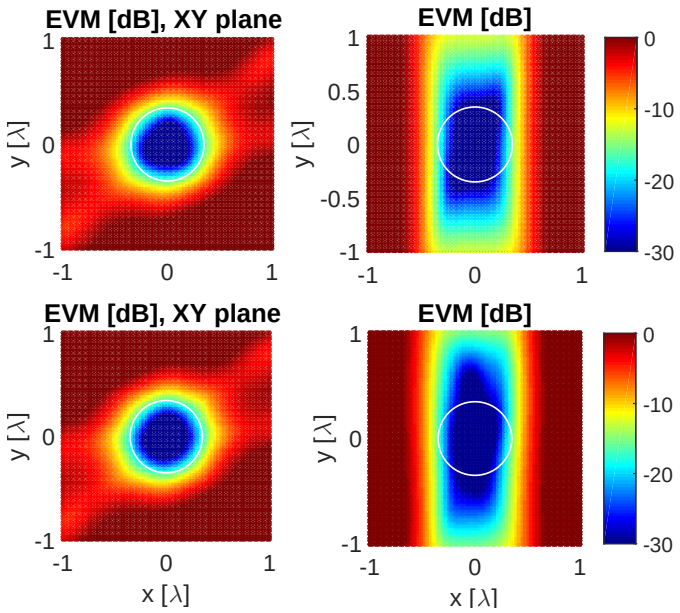

Figure 8. EVM for a ray with AoA = 22.5^o and EoA = 0^o. Top: Scenario A. Bottom: Scenario B. Left: azimuth plane. Right: plane perpendicular to the impinging ray direction.

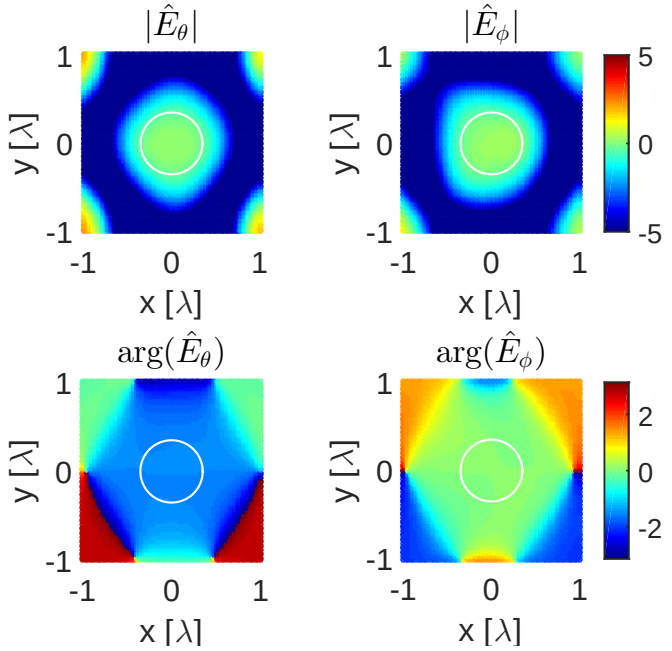

Figure 9. $\hat{E_\theta}$ and $\hat{E_\phi}$ with AoA = 22.5^o and EoA = 15^o on the plane perpendicular to the impinging ray direction. Top: Field strength [dB]. Bottom: phase [rad].

(i.e. between Rx position 10 and 20), dominant rays imping from a AoAs around 0^o and EoAs around 0^o. In route 1, the EoA angle is relatively low, i.e. ranged from -10^o to 10^o, whereas in route 2 the elevation angle ranges from -30^o to 30^o.

2) VDT in MPAC setups: Configuration P2 is used for reproducing the RT simulated channels along the two routes. Note that the EVM values are calculated from the samples over the test zone surface. As explained in Section III-C, each

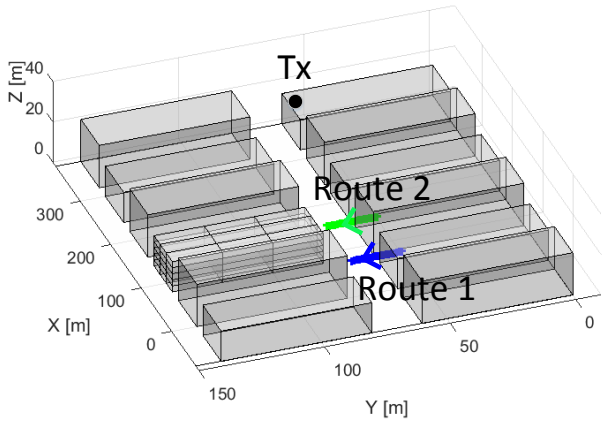

Figure 10. Scenario for RT simulations. The Tx is a vertically polarized isotropic antenna, placed at 17m height. Transmit power is 5 dBm and the simulation frequency is 2 GHz. Rx positions are placed at 1.5 m height.

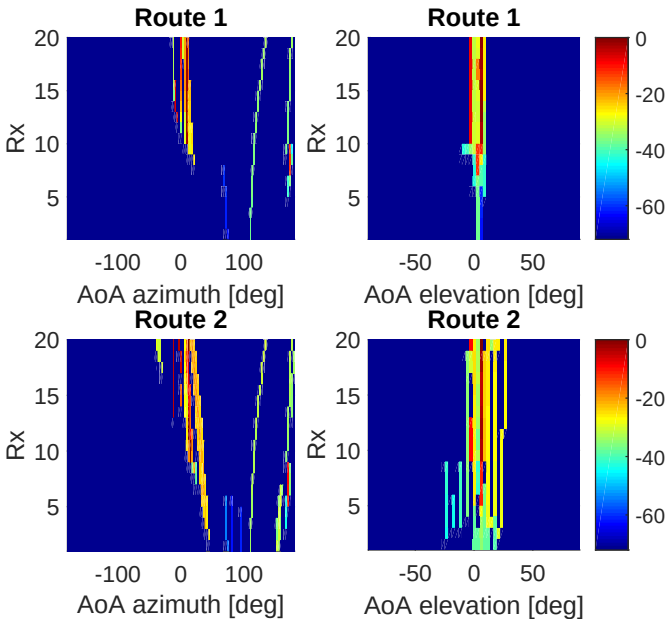

Figure 11. Power angular spectrum for the RT simulation. Left: azimuth. Right: elevation.

ray is optimized individually. The rms EVM values for all rays along the two routes are shown in Figure 12. Note that at different Rx positions there might be different number of rays, as a limited power range is set in RT simulation to reduce the computation time. For Route 1, where the range of the elevation angles was lower, rms EVM values up to around -17dB are observed. On the other hand, Route 2 shows rms EVM values up to -10 dB, due to the higher elevation range observed in this route. Note that the probe configuration and number of probes can be optimized for different scenarios to improve the emulation accuracy [23].

V. Measurement Verification

A. Measurement Setup

Measurements validating the field synthesis technique have been reported in the literature before. First measurement

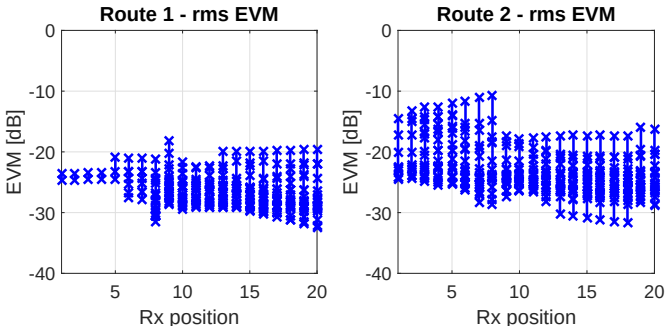

Figure 12. Rms EVM values for the rays over the two routes.

Figure 13. A photo of the practical 3D MPAC setup in the measurement. The chamber size is 6.0 m x 6.0 m x 5.8 m and the distance from the probes to the center is 2.2 m. There are 16 probes in elevation 0^o with 22.5^o azimuth spacing, 8 probes in elevation $+30^o$ with 45^o azimuth spacing and 8 probes in elevation -30^o with 45^o azimuth spacing. There was no azimuth angle offset between the three rings. Note that a Satimo sleeve dipole was used to scan the field in the measurements.

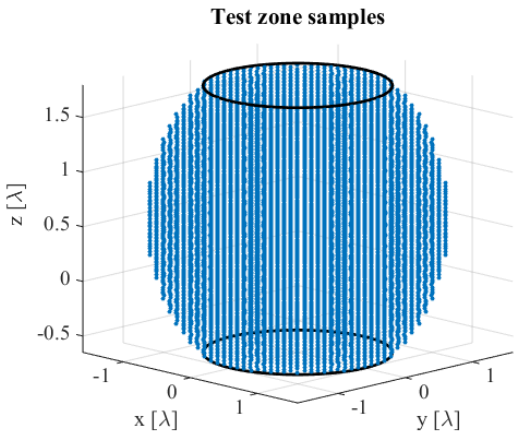

Figure 14. Measurement positions. The measurement positions are bounded by an sphere (radius 1.6λ) with spherical caps of height 0.4λ cut off in the up and low parts in the z axis.

validation of a plane wave using a seven-element Yagi-Uda antennas was reported in [20]. Excellent agreement of the complex amplitude between measurements and theoretical values was achieved. However, the work was limited to create a single plane wave from a specific direction. In [27], measurements in a preliminary 2D MPAC setup were performed, where 2D vertically polarized plane waves were synthesized and measured. Promising match between measured and simulated fields was observed, yet the results suffered from system non-idealities, e.g. cable effects [27]. In [28], a measurement campaign using commercial 2D MPAC setups was performed. The accuracy obtained in [28] was better than in [27] because chokes/cartridges and ferrite loaded cables were used to reduce cable effects. Preliminary results validating field synthesis were reported in [29] for a 2D MPAC setup. Measurement results reported in the literature have been generally limited to 2D setups, and scanning of a 2D test zone. In this section, we describe extensive measurements that were performed to validate field synthesis algorithms in a practical 3D MPAC setup, where a 3D test zone was scanned. To the authors' best knowledge, there are no prior reports on field synthesis validation in practical 3D MPAC setups. The goal of the measurement campaign is to check whether the 3D MPAC system works as expected. This is a first step to achieve VDT via replaying RT simulated channels using the field synthesis technique.

The measurement system is illustrated in Figure 3. The 3D probe configuration constructed for the measurement campaign is shown in Figure 13. The measurement system consisted of four Propsim F8 channel emulators, a vector network analyzer (phase/amplitude receiver). The probe antennas were absorber nested dual polarized Vivaldi antennas (ETS-Lingren's 3165-01) as illustrated in the figure. A sleeve dipole antenna and a magnetic loop antenna from Satimo were used for calibration purposes at 2450 MHz. A series of measurements were performed at 2450 MHz. The vertically polarized port of each probe is connected to one output port of a Propsim F8, where appropriate complex weights can be set. The calibration dipole (with central frequency 2450 MHz) was used in the measurement campaign to scan the electrical field over the test zone samples shown in Figure 14. The measurement positions are uniformly distributed in the test zone as depicted in Figure 14. Measurement positions are separated 0.1λ in x, y and z axes directions. The scanned volume is ranged -1.6λ to 1.6λ in x and y axis directions and -0.63λ to 1.77λ (i.e. 2.4λ range) in z axis directions, resulting in a total of 15957 measurement positions. At each measurement position, the amplitude and phase were recorded. A complete scan of the test volume took 22 hours and 39 minutes, meaning that the measurement time at each position was around 5 seconds. The measurement grid was unfortunately not symmetric in z axis (i.e. around 0.57λ shifted in $+z$ axis direction).

B. *Target field*

In the measurements reported in the literature, often a plane wave with an arbitrary impinging angle or a collection of plane waves were targeted. As a result, the probes located closer to target wave direction are dominant in the synthesized field, while others have a negligible contribution [20], [29]. In the measurement campaign, two representative target fields were considered.

- 2D case: A omni-directional field impinging from the azimuth plane (i.e. uniformly distributed plane waves on

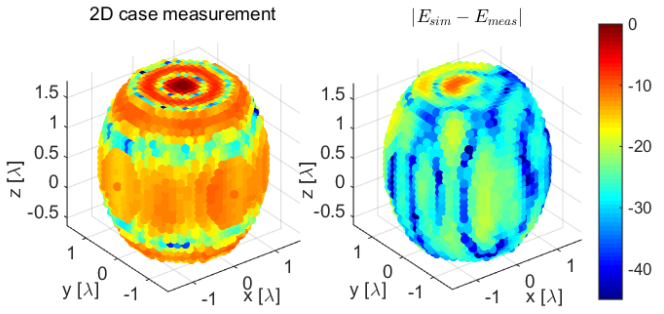

Figure 15. Measured field strengths (left) and deviation between measurement and simulation (right) over the 15957 grid points for the 2D case.

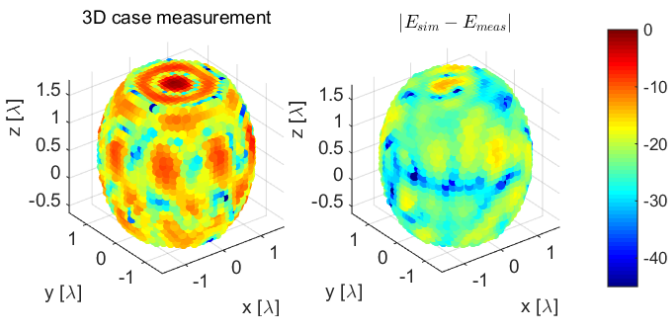

Figure 16. Measured field strengths (left) and deviation between measurement and simulation (right) over the 15957 grid points for the 3D case.

the azimuth plane with same complex amplitude). In this case, only the 16 probes on the azimuth plane were active. The probes on other elevation rings were terminated with 50 Ω to avoid cable reflections.

- 3D case: Omni-directional fields impinging from three elevations planes with elevation angles -30^o, 0^o and 30^o. In this case, all 32 probes were active.

The probe weights for the two considered cases can be obtained via field synthesis techniques discussed in Sec III.C. Simulation results showed that probes are weighted with same complex amplitude, as expected. And hence we can check whether all RF chains connected to the probes are working properly and can be accurately controlled under these two cases. Note that a plane wave with an arbitrary impinging angle or multiple plane waves can be targeted as well, since the field synthesis principle and measurement procedure would work the same. Measurements with non-uniform target field, e.g. a plane wave or multiple plane waves, are unfortunately not included in the paper due to the measurement time and complexity.

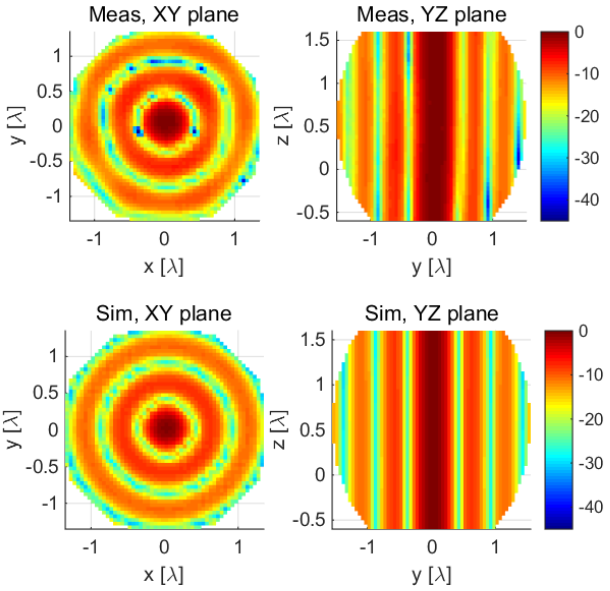

Figure 17. Measured and simulated field strengths over the xy plane (left figures) and yz plane (right figures) for the 2D case.

C. Experimental results and comparisons with theory

The field strength measured over the measurement grid for the 2D case is shown in Figure 15 (left). The results are normalized to the maximum value over all the points. To investigate how well the amplitude and phase of the electric field is reproduced, the deviation between the measured field and simulated field is calculated and plotted in Figure 15 (right). Good agreement between the measured and simulated complex field is achieved, with a maximum deviation of -10dB and a mean deviation of -22dB over all grid points. Similarly, the measured field strength and deviation between measurement and simulation are shown in Figure 16 for the 3D case. The electrical field is well reproduced as well, with a maximum deviation of -11dB and mean deviation of -22dB between the measured and simulated field. The deviation between measurement and simulation is caused by measurement uncertainties present in the practical setup.

To gain more insight into the results, the measured and simulated field strengths over xy and yz plane for the 2D and 3D case are shown in Figure 17 and Figure 18, respectively. Generally, very good agreement between the simulation and measurement can be seen for both cases. Field strength distributions over the xy plane follow a 2D Bessel function distribution for the 2D case, as expected. Over the yz plane, the field strength follows a Bessel function along the y axis. The field strength in the z axis direction is constant, since the waves radiated from the probes are planar and they are in parallel to the xy plane. For the 3D case, the field strength in z axis varies, due to the waves radiated from the two elevation rings.

Field strength over the x, y and z axis directions are shown in Figure 19. For the 2D case, the target field is calculated assuming omni-directional field impinging from the azimuth plane (2D). For the 3D case, the target field is obtained assuming omni-directional field impinging from three planes with elevation angles -30^o, 0^o and 30^o respectively. The simulated fields match well with the target fields within a range of $[-2\lambda, 2\lambda]$ over x, y and z axis directions and deviates outside this range for the 2D case, due to the fact that a limited number of probes in a size limited OTA setup (radius 2 m) are utilized. The measured field match well with the simulation and target, with a small deviation over the z axis. For the 3D case, excellent agreement is achieved between the simulated and measured and target fields over the three axis directions.

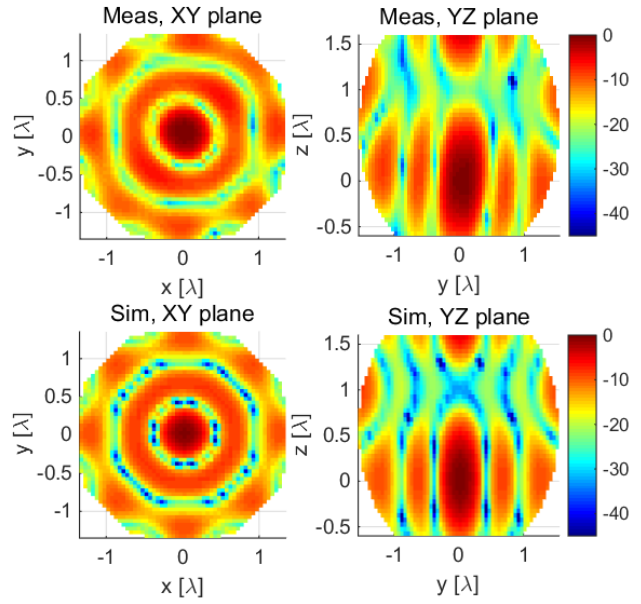

Figure 18. Measured and simulated field strengths over the xy plane (left figures) and yz plane (right figures) for the 3D case.

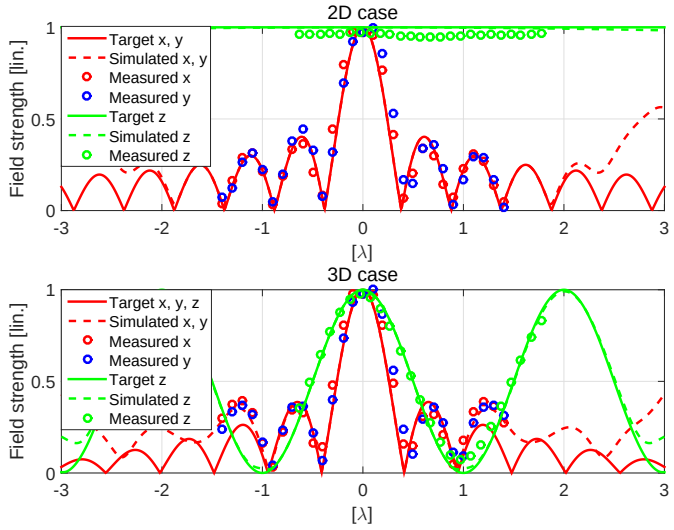

Figure 19. Target, measured and simulated field strength over the x, y and z axis directions for the 2D (top) and 3D (bottom) case.

VI. Conclusions and Future Work

A field synthesis technique has been proposed to replay ray tracing simulated channels in the MPAC setups in order to achieve VDT in a laboratory environment in this paper. The field synthesis algorithm to reproduce a ray with an arbitrary polarization and impinging angle in 3D MPAC setups is firstly detailed and then it is applied to emulate realistic RT simulated channels. Simulation results show that RT simulated channels can be reproduced in a 3D MPAC setup with 16 probe antennas with reasonable accuracy, i.e. rms EVM up to -17dB for a RT channel with low elevation angles and -10 dB for a RT channel with high elevation angles. A practical 3D MPAC setup was constructed and tested in an anechoic chamber at 2450 MHz to verify the field synthesis algorithm and gain experience in practical setups. The agreement between measurement and simulation was excellent for the complex electrical field, with a mean deviation up to -20 dB for the 2D case and -22dB for the 3D case. The feasibility of performing VDT with the field synthesis technique is supported by the measurement results.

There are a number of logical extensions to this topic left for future work. Different probe configurations could be investigated to improve the results and to increase the size of test zone. More realistic scenarios (e.g. database of a real city with known base station antennas and drive test routes) could be used and the results could be compared with channel sounding measurements. In the measurement, the probe antennas could be dual-polarized and a magnetic loop could be used to scan the test zone. Furthermore, throughput testing of MIMO capable terminals under various reproduced channels in MPAC setups could be performed.

Acknowledgment

This work has been supported by the Danish High Technology Foundation via the VIRTUOSO project. The authors appreciate the assistance provided by Verkotan Oy in the practical measurements. The authors would like to thank Dr. Vittorio Degli-Esposti and Dr. Enrico Maria Vitucci for providing the "3D Scat" ray tracing tool.

Wei Fan received his Bachelor of Engineering degree from Harbin Institute of technology, China in 2009, Master's double degree with highest honours from Politecnico di Torino, Italy and Grenoble Institute of Technology, France in 2011, and Ph.D. degree from Aalborg University, Denmark in 2014. From February 2011 to August 2011, he was with Intel Mobile Communications, Denmark as a research intern. He conducted a three-month internship at Anite telecoms oy, Finland in 2014. His main areas of research are over the air testing of MIMO terminals, radio channel modelling and virtual drive testing.

Ines Carton received her Bachelor degree in telecommunications engineering from the University of Oviedo (Spain) in 2013. She received her M.Sc. in Wireless Communication Systems from Aalborg University (Denmark) in 2014, where she completed her Master Thesis in collaboration with Intel Mobile Communications (Denmark). Currently, she is employed at the Department of Electronic Systems at Aalborg University as a research assistant. The focus of her research is on MIMO OTA testing and channel modeling.

Pekka Kyösti holds M.Sc. in mathematics from Oulu University, Finland. From 1998 to 2002 he was with Nokia Networks working on the field of transceiver baseband algorithms and signal processing. From 2002 to 2013 he was with Elektrobit, Oulu. Since 2002 he has been working on radio propagation, channel measurements and modelling. He has participated in the channel modelling work in European METIS 2020 project, IST-WINNER projects and NEWCOM network of excellence since 2004. He contributes actively to scientific conferences and COST actions. He was moved to Anite along the acquisition in January 2013. Currently his responsibilities are channel modelling for 5G and MIMO OTA research in Anite.

Gert Frølund Pedersen was born in 1965 and married to Henriette and have 7 children. He received the B.Sc. E. E. degree, with honour, in electrical engineering from College of Technology in Dublin, Ireland in 1991, and the M.Sc. E. E. degree and Ph. D. from Aalborg University in 1993 and 2003. He has been with Aalborg University since 1993 where he is a full Professor heading the Antenna, Propagation and Networking LAB with 36 researcher. Further he is also the head of the doctoral school on wireless communication with some 100 phd students enrolled. His research has focused on radio communication for mobile terminals especially small Antennas, Diversity systems, Propagation and Biological effects and he has published more than 175 peer reviewed papers and holds 28 patents. He has also worked as consultant for developments of more than 100 antennas for mobile terminals including the first internal antenna for mobile phones in 1994 with lowest SAR, first internal triple-band antenna in 1998 with low SAR and high TRP and TIS, and lately various multi antenna systems rated as the most efficient on the market. He has worked most of the time with joint university and industry projects and have received more than 12 M$ in direct research funding. Latest he is the project leader of the SAFE project with a total budget of 8 M$ investigating tunable front end including tunable antennas for the future multiband mobile phones. He has been one of the pioneers in establishing Over-The-Air (OTA) measurement systems. The measurement technique is now well established for mobile terminals with single antennas and he was chairing the various COST groups (swg2.2 of COST 259, 273, 2100 and now ICT1004) with liaison to 3GPP for over-the-air test of MIMO terminals. Presently he is deeply involved in MIMO OTA measurement.

REFERENCES

[1] Anite, "Virtual drive testing toolset," February 2015. [Online]. Available: http://www.anite.com/virtualdrivetesting

[2] A. S. Erik Org, "Field-to-lab infuses the real world into mobile-device virtual testing," December 2011. [Online]. Available: http://mobiledevdesign.com/learning-resources/field-lab-infuses-real-world-mobile-device-virtual-testing-0

[3] Spirent, "Spirent virtual drive test (VDT)-conversion tool," February 2015. [Online]. Available: http://www.spirent.com/Products/Virtual_Drive_Testing

[4] "Verification of radiated multi-antenna reception performance of User Equipment," 3GPP, TR 37.977 V1.0.0, Sep. 2013.

[5] W. Fan, X. Carreño, P. Kyösti, J. Ø. Nielsen, and G. F. Pedersen, "Over the air testing of MIMO capable terminals: Capabilities and challenges of multi-probe anechoic chamber method," *IEEE Vehicular Technology Magazine*, 2015.

[6] R. K. Sharma, W. Kotterman, M. H. Landmann, C. Schirmer, C. Schneider, F. Wollenschläger, G. D. Galdo, M. A. Hein, and R. S. Thomä, "Over-the-air testing of cognitive radio nodes in a virtual electromagnetic environment," *International Journal of Antennas and Propagation*, vol. 2013, 2013.

[7] P. Kyösti, T. Jämsä, and J.-P. Nuutinen, "Channel modelling for multiprobe over-the-air MIMO testing," *International Journal of Antennas and Propagation*, vol. 2012, 2012.

[8] J. Reed, "Emulation and controlled testing of MIMO OTA channels," Mar. 31 2015, uS Patent 8,995,511. [Online]. Available: https://www.google.dk/patents/US8995511

[9] "Spatial channel model for Multiple Input Multiple Output (MIMO) simulations," 3GPP, TR 25.996 V12.0.0, Sep. 2014.

[10] P. Kyösti, "Radio channel data and the use thereof," Aug. 15 2013, uS Patent App. 13/371,960. [Online]. Available: http://www.google.com/patents/US20130210474

[11] J. Toivanen, T. Laitinen, V. Kolmonen, and P. Vainikainen, "Reproduction of arbitrary multipath environments in laboratory conditions," *Instrumentation and Measurement, IEEE Transactions on*, vol. 60, no. 1, pp. 275–281, Jan 2011.

[12] F. Fuschini, H. El-Sallabi, V. Degli-Esposti, L. Vuokko, D. Guiducci, and P. Vainikainen, "Analysis of multipath propagation in urban environment through multidimensional measurements and advanced ray tracing simulation," *Antennas and Propagation, IEEE Transactions on*, vol. 56, no. 3, pp. 848–857, March 2008.

[13] V. Degli-Esposti, D. Guiducci, A. de'Marsi, P. Azzi, and F. Fuschini, "An advanced field prediction model including diffuse scattering," *Antennas and Propagation, IEEE Transactions on*, vol. 52, no. 7, pp. 1717–1728, July 2004.

[14] P. Almers, E. Bonek, A. Burr, N. Czink, M. Debbah, V. Degli-Esposti, H. Hofstetter, P. Kyö, D. Laurenson, G. Matz *et al.*, "Survey of channel and radio propagation models for wireless MIMO systems," *EURASIP Journal on Wireless Communications and Networking*, vol. 2007, 2007.

[15] V. Degli-Esposti, F. Fuschini, E. Vitucci, and G. Falciasecca, "Measurements and modelling of scattering from buildings," *Antennas and Propagation, IEEE Transactions on*, vol. 55, no. 1, pp. 143–153, January 2007.

[16] P. Hallbjorner, J. Sanchez-Heredia, P. Lindberg, A. Martinez-Gonzalez, and T. Bolin, "Multipath simulator measurements of handset dual antenna performance with limited number of signal paths," *Antennas and Propagation, IEEE Transactions on*, vol. 60, no. 2, pp. 682–688, Feb 2012.

[17] K. Sakaguchi, T. Sakata, and A. Yamamoto, "Performance evaluation of spatial correlation characteristics for handset antennas using spatial fading emulator based on Clarke's model," *IEICE transactions on communications*, vol. 93, no. 10, pp. 2514–2522, 2010.

[18] O. Bucci, M. Migliore, G. Panariello, and D. Pinchera, "Plane-wave generators: Design guidelines, achievable performances and effective synthesis," *Antennas and Propagation, IEEE Transactions on*, vol. 61, no. 4, pp. 2005–2018, April 2013.

[19] R. Haupt, "Generating a plane wave with a linear array of line sources," *Antennas and Propagation, IEEE Transactions on*, vol. 51, no. 2, pp. 273–278, Feb 2003.

[20] D. Hill and G. Koepke, "A near-field array of yagi-uda antennas for electromagnetic-susceptibility testing," *Electromagnetic Compatibility, IEEE Transactions on*, vol. 28, no. 4, pp. 170–178, Nov 1986.

[21] W. Kotterman, C. Schirmer, M. Landmann, and G. Del Galdo, "On arranging dual-polarised antennas in 3D wave field synthesis," in *Antennas and Propagation (EuCAP), 2014 8th European Conference on*, April 2014, pp. 3406–3410.

[22] C. Schirmer, M. Landmann, W. Kotterman, M. Hein, R. Thoma, G. Del Galdo, and A. Heuberger, "3D wave-field synthesis for testing of radio devices," in *Antennas and Propagation (EuCAP), 2014 8th European Conference on*, April 2014, pp. 3394–3398.

[23] P. Kyösti and A. Khatun, "Probe configurations for 3D MIMO over-the-air testing," in *Antennas and Propagation (EuCAP), 2013 7th European Conference on*, April 2013, pp. 1421–1425.

[24] J. E. Hansen, *Spherical near-field antenna measurements*. Iet, 1988, vol. 26.

[25] M. D'Urso, G. Prisco, and M. Cicolani, "Synthesis of plane-wave generators via nonredundant sparse arrays," *Antennas and Wireless Propagation Letters, IEEE*, vol. 8, pp. 449–452, 2009.

[26] A. Buonanno, M. D'Urso, and G. Prisco, "Reducing complexity in indoor array testing," *Antennas and Propagation, IEEE Transactions on*, vol. 58, no. 8, pp. 2781–2784, Aug 2010.

[27] W. Fan, X. Carreño, J. Ø. Nielsen, K. Olesen, M. Knudsen, and G. F. Pedersen, "Measurement verification of plane wave synthesis technique based on multi-probe MIMO-OTA setup," in *Vehicular Technology Conference (VTC Fall), 2012 IEEE*, Sept 2012, pp. 1–5.

[28] W. Fan, I. Szini, M. Foegelle, J. Ø. Nielsen, and G. F. Pedersen, "Measurement uncertainty investigation in the multi-probe OTA setups," in *Antennas and Propagation (EuCAP), 2014 8th European Conference on*, April 2014, pp. 1068–1072.

[29] W. Kotterman, C. Schirmer, M. Lorenz, R. Damm, G. Galdo, A. Heuberger, and M. Landmann, "A Calibration Procedure for Practical Wave-Field Synthesis in Over-The-Air Testing," May 2015, tD(13)07054.